ENHANCING BIOMEDICAL IMAGE CLASSIFICATION: EXPLORING VARIOUS CLASSIFIERS FOR ACCURATE ANALYSIS

Abstract

The primary focus of this study revolves around enhancing disease diagnosis, analysis, and detection through optimized models, particularly for biomedical images. In the medical field, professionals heavily rely on pathological reports for diagnosis. However, visualizing these reports can greatly aid doctors in their diagnostic process. This research specifically aims to develop a streamlined model for swift analysis and diagnosis. The study encompasses data related to Brain Tumors, Skin Cancer, Liver Disorders, and Breast Cancer.

The methodology involves several steps: starting from raw data, utilizing Convolutional Neural Networks (CNNs) for image data, extracting features from the data, and optimizing these features for machine learning models. The machine learning algorithms employed in this research include the k-nearest neighbors' algorithm (KNN), Random Forest (RF), and Support Vector Machine (SVM). These algorithms are evaluated across all cancer types under consideration.

Distinct accuracies are observed from different machine learning classifiers. Notably, CNN, unlike other models, does not rely on external features due to its intrinsic capability for feature extraction, selection, and integration. On the other hand, for the other machine learning techniques, feature acquisition is crucial for the classifier model.

In certain cases of cancer data, Support Vector Machine (SVM)

Authors

Jaya Bijaya Arjun Das
Computer Science and Engineering
ITER, SOA University
Bhubaneswar, Odisha, India.
jbadas1999@gmail.com

Debasmita Behera
Computer Science and Engineering
ITER, SOA University
Bhubaneswar, India
debasmitabehera148@gmail.com

demonstrates higher accuracy, while CNN performs best when external features are not utilized. Interestingly, through the process of Brain Storm Optimization (BSO), optimizing features and applying them to the SVM model yields exceptional results compared to alternative methods.

Keywords: Biomedical images, cancer, KNN, SVM, Random Forest, ABCD rule, Feature extraction, BSO

I. INTRODUCTION

Biomedical image processing is an intriguing and swiftly evolving field driven by the advancements in image processing techniques, encompassing tasks like image analysis, recognition, and enhancement. "Medical image processing" pertains to the utilization of computers to manage medical images, yielding benefits for surgeons, physicians, and patients alike. Medical imaging involves capturing images from a living organism's body for medical purposes, facilitating disease identification and study. This technique aids in the early detection and treatment of fractures, infections, and diseases, especially those lacking noticeable symptoms. The amalgamation of hardware devices and image processing techniques in medical equipment has significantly propelled the medical sector forward. Diagnostic imaging notably enhances patient outcomes and empowers clinicians with expedient and reliable information. It also enhances surgical precision and accuracy. Digital images offer multiple advantages, such as swift processing, low costs, quality preservation during duplication, convenient storage and sharing, and adaptable manipulation. Nevertheless, drawbacks include potential copyright issues, challenges in resizing without quality loss, high memory requirements, and the need for robust CPUs for manipulation. Common imaging methods encompass Digital X-rays, Computerized Tomography (CT scans), Ultrasound, and Magnetic Resonance Imaging (MRI).

Medical images, like magnetic resonance imaging (MRI), ultrasound, computed tomography (CT), and mammography, often encounter various levels of noise due to factors such as transmission and processing [12]. Numerous factors contribute to image corruption during transmission or acquisition in the field of image processing, leading to degraded image content due to noise [12]. To restore the original information in images and eliminate noise, specific denoising techniques are employed. These methods involve applying a kernel that convolves across the image, resulting in a noise-free image post-convolution. The size of the kernel (window) varies, as does the desired outcome. Among the commonly used techniques, median filtering stands out [6]. Median filtering is effective when image noise density is low, but its performance diminishes under high noise density. To address this issue, spatial filtering can be employed [13]. An example of such a filtering approach is the adaptive median filter [19], which improves upon median filtering by utilizing a two-step process. The significant advantage of the adaptive median filter lies in its adaptability to the image's characteristics during filtering [7]. Furthermore, the adaptive filter excels not only in handling impulse noise but also speckle noise and Gaussian noise [8].

Currently, medical image analysis plays a critical role in modern medical science. Computer-aided diagnostic (CAD) methods are essential for understanding disease mechanisms, as interpreting medical images directly can be challenging. Machine learning has significantly contributed to this field. Various types of medical image datasets are available, each containing both normal and abnormal instances. Examples include skin cancer, brain tumors, chest X-rays, and CT scans. These datasets are commonly used for classification tasks.

In medical image analysis, the application of machine learning is highly advantageous. The first step involves extracting useful features from the images, which is achieved through different feature extraction algorithms. Once features are extracted, classification is performed using diverse machine learning algorithms such as Support Vector

Machines, Decision Tree Classifiers, Random Forests, and K-Nearest Neighbors. However, classifying medical datasets is challenging due to their large instance and feature counts. The outcome of classification heavily relies on the chosen features. Achieving high classifier accuracy demands a well-curated feature set. When datasets are too small, there might be insufficient features for description, whereas excessively large datasets could diminish feature impact.

Recent reports indicate that brain tumors are considered the most perilous and lethal among all tumor types. These tumors exhibit uncontrolled growth within the brain, potentially leading to abnormal brain activity and the deterioration of healthy nerve cells [35]. Consequently, essential functions like speech, cognition, and movement might be compromised. Recognized as a critical form of cancer, brain tumors can be effectively treated if detected early, often through close monitoring by neurosurgeons. These tumors manifest as masses developing within the brain, which can impact brain or skull tissues. They are categorized into benign, non-cancerous tumors, and malignant, cancerous tumors that infiltrate brain cell boundaries [36]. The irregular growth of these tumors in the brain often results in elevated pressure.

Magnetic Resonance Imaging (MRI) stands out as a superior technique for visualizing brain tumor images [37]. MRI offers more precise results compared to CT scans in tumor identification. This explains the preference of most neurosurgeons for MRI images in patient diagnoses. However, manual detection of brain tumors from MRI images remains a demanding and time-consuming task, relying heavily on the doctor's availability and diagnostic experience. To mitigate these challenges, automated systems have been developed to reduce the reliance on human expertise and enhance brain tumor classification. Numerous computer-aided diagnostic systems have been devised, yielding promising outcomes [38].

In the present era, the Information Technology (IT) industry has witnessed a substantial demand for Deep Learning, a subset of machine learning inspired by neural networks that enables computers to mimic human-like behavior. Deep Learning encompasses various models, including Autoencoders, Recurrent Neural Networks (RNN), and Artificial Neural Networks (ANN). Notably, Convolutional Neural Networks (CNNs) have significantly contributed to computer vision and image analysis. CNNs are especially adept at analyzing and classifying visual images and have found applications in medical image analysis [39], computer vision [40], natural language processing [41], and image and video recognition [42].

Cancer poses one of the greatest challenges in modern medicine. It emerges when cells within a specific part of the body begin to grow uncontrollably [57]. These cancerous cells outcompete normal cells for nutrients, weakening and causing the demise of healthy cells. Consequently, this weakens the immune system and can lead to overall body weakness. Over time, these malignant cells can spread throughout the body, affecting organs such as the liver, bones, breasts, lungs, bladder, and skin [60].

The skin, the body's largest organ, consists mainly of seven layers of ectodermal tissues that safeguard internal organs [58]. Among its functions are temperature regulation, sensation of touch, cold, and heat, as well as protection against external elements and microbes. When an area of the skin becomes abnormal compared to its surroundings, it is

referred to as a skin lesion. Typically, skin lesions arise due to infections, whether internal or external. These lesions are categorized as either primary or secondary, and they can potentially develop into skin cancer [58].

Skin cancer arises from abnormal cells that infect the human body. Early detection is crucial to prevent the cancer from spreading [57]. In India, over 5000 skin cancer patients are hospitalized annually, with approximately 4000 resulting in death [58]. To aid in detecting skin lesions, various automated techniques have been developed to ensure accuracy, efficiency, and performance. Skin tumors can be classified as Basal Cell Carcinoma (BCC), Squamous Cell Carcinoma (SCC), and Melanoma. The malignancy of these tumors depends on their rate of growth and spread; if they spread, they are considered malignant, whereas those confined to a region are benign. Manual detection of skin cancer is inadequate since naked-eye inspection might overlook crucial features, potentially leading to incorrect treatment and fatalities. Timely identification of skin cancer through automated methods significantly enhances accuracy and efficiency [59].

However, automated skin lesion detection encounters challenges such as artifacts, low contrast, skin tone variations, hair, veins, and the visual similarity between melanoma and non-melanoma cases. These issues can be mitigated using preprocessing techniques. Preprocessed images undergo segmentation to accurately isolate the skin lesion. Multiple segmentation methods are employed, including basic global thresholding, the watershed algorithm, wavelet algorithms, Otsu's method, active contours, and more. Following segmentation, the segmented skin lesion image is subjected to feature extraction using techniques like CASH rule, ABCD rule, ABCDE rule, GLCM, HOG, LBP, and HLIFS [58]. Harmful rays like ultraviolet light from sun exposure are a primary cause of melanoma [59]. Researchers globally have attempted traditional methods to combat this deadly disease, but obstacles like high costs, sustainability of traditional telemedicine, and limited expert availability have hindered progress. It's worth noting that 90% of cases result from exposure to UV radiation from the sun [61].

II. RELATED LITERATURE

Biomedical image processing is a rapidly expanding field encompassing signal acquisition, image formation, segmentation, processing, denoising, and representation for medical diagnosis based on visual attributes. This area involves the analysis of medical images like MRI, CT, ultrasound, and microscopy, generating substantial data that needs efficient extraction and presentation. This review section addresses the fundamentals and applications of biomedical image processing, discussing techniques such as deblurring, noise reduction, filtering, analysis, and texture assessment, with illustrative examples.

Numerous methods are employed to enhance medical image clarity for improved patient diagnosis. Various median filtering techniques are proposed and examined, mainly suitable for images with low noise density. Comparisons of filtered images rely on metrics like Mean Square Error (MSE) and Peak Signal to Noise Ratio (PSNR). Standard median filters serve as the simplest type. Impulsive noise removal is achieved through decision-based approaches that aim to retain image features while suppressing noise. Adaptive decision-based median filtering, particularly for noise densities up to 50%, can offer better visual quality and PSNR values. A self-adaptive median filter that utilizes local pixel distribution is

introduced for eliminating salt and pepper noise. Methods using thresholds and standard medians are employed to detect noise and substitute original pixel values with those closer to the median. Novel techniques, such as ranked-order based adaptive median filters, cater to different impulse noise types, featuring variable window sizes for noise reduction and sharpness preservation. Spatial domain approaches involving overlapping windows and effective median selection are proposed for impulse noise-corrupted images, minimizing distortions.

A novel computer-aided diagnosis system is presented to differentiate normal from abnormal images. Structural feature extraction involves LBP and HOG methods, with PSO used to determine the best feature set. SVM classification with 10-fold cross-validation is employed. Experiments on medical datasets, including Breast Cancer, Heart Stat log, and Dermatology datasets, demonstrate the efficacy of PSO CFS filtering in enhancing classifier accuracy. The proposed PSO wrapper method yields the highest accuracy. A new algorithm, BPSO+C4.5, is introduced for classifying high-dimensional data without requiring extensive population size or iterations, performing well across dimensional datasets.

In reference [23], a stochastic genetic algorithm was introduced by the authors to optimize the parameters of Support Vector Machines (SVM). Their experimentation was conducted on a small dataset, revealing that their approach outperformed existing classification methods in terms of accuracy. The primary focus of this work was on optimizing the kernel parameters of SVM. Moving to reference [24], the authors presented the BSOA (Brain Storm Optimization Algorithm), designed for feature selection in input datasets and parameter tuning of SVM. They conducted experiments using three medical datasets to validate their approach's effectiveness. In [25], a pair of novel multimodal Particle Swarm Optimization (PSO) algorithms, namely MNPSO-C and MNPSO-S, were introduced. Comparative studies on various Feature Selection benchmarks illustrated that these algorithms could identify multiple sets of feature solutions while maintaining classification accuracy.

The content of [26] described three distinct feature selection methods proposed to enhance classification outcomes. The study focused on the PIMA Indian diabetes dataset, utilizing metaheuristic algorithms such as Genetic Algorithm (GA), Particle Swarm Optimization (PSO), and K-means clustering for selecting relevant input features. The classification task was performed using the K-nearest neighbors (KNN) classifier. Addressing [27], a new algorithm named Brain Storm Optimization (BSO) algorithm was put forth by the author, drawing inspiration from human brainstorming processes. Efficiency evaluation was conducted using two benchmark functions: the unimodal Sphere function and the multimodal Rastrigin function. The BSO algorithm was tested with dimensions 10, 20, and 30, utilizing k-means clustering to partition individuals into clusters.

In [28], two modified versions of the BSO algorithm were introduced. The first modification incorporated a grouping-based model in the grouping operator, while the second involved an idea difference strategy (IDS) replacing the Gaussian random strategy in the generating operator. The authors applied k-means clustering initially and introduced Gaussian noise afterward. The content of [29] proposed a hybrid feature selection model, PCA-IG, using the Breast Cancer Dataset. The authors demonstrated that feature selection could enhance accuracy and other performance metrics. The J48 decision tree classifier, when

coupled with PCA-IG, exhibited superior performance. Describing [30], the authors presented an optimized image segmentation approach utilizing Genetic Fuzzy C-Means (GFCM) with genetic algorithm optimization. The results showcased the method's utility in medical image analysis. In [31], the author used a novel method, WCA+DCCN, for brain tumor classification employing the brain tumor dataset. The approach involved wavelet transform for image segmentation.

Reference [32] detailed the utilization of a fuzzy classifier integrated with deep learning techniques for medical image classification. The method outperformed state-of-the-art approaches in terms of accuracy. [33] employed the Breast Cancer dataset to detect cancerous regions using gene expression and deep learning models.

In recent years, the potential of Convolutional Neural Networks (CNNs) in the medical field has expanded. Computer-aided diagnostic systems enable disease detection, diagnosis, and classification, mainly relying on medical images like MRI, CT scans, and X-rays. A novel approach [35] utilized a clustering-based CNN and Fuzzy C-Means (FCM) for automated brain tumor detection, a critical step in preventing brain tumor-related deaths. In [36], an automated system for brain tumor detection and localization from Brain MRI images was introduced. CNN architecture played a key role in image classification, with data augmentation handling pre-processing and morphological-based segmentation addressing segmentation in the final step. In the field of neuroscience, deep learning methods play a crucial role in diagnosing diseases. In the context of brain tumor classification, a study (reference [38]) presented a CNN-based approach consisting of three layers, achieving outcomes within 35 epochs. This technique involved preprocessing steps that enabled the differentiation of tumor and non-tumor regions in brain MRI scans.

A different study (reference [43]) in the same field introduced a Deep Convolutional Neural Network (DCNN) model combined with the Sine Cosine Algorithm (WCA) for brain tumor detection. This method utilized discrete wavelet transforms (DWT) and transform segmentation to enhance tumor identification through discrete wavelets. The results indicated that this DCNN+WCA model outperformed other methods discussed in the study. Similarly, in a separate work (reference [44]), a CNN-based algorithm was proposed for pneumonia detection in chest X-ray images. In the realm of brain MRI image classification (reference [51]), a DNN model was employed, incorporating discrete wavelet transforms (DWT) and principal components analysis (PCA) alongside the classifier. Another study (reference [54]) introduced a DNN model specifically for MRI-based tumor segmentation. This model was composed of seven layers, including three convolutional layers, three ReLU layers, and a SoftMax layer.

Addressing the manual diagnosis of brain tumors using MRI images, a study (reference [45]) suggested utilizing five pre-trained models (AlexNet, Vgg-16, ResNet-18, ResNet-34, and ResNet-50) for automated classification. Among these, ResNet-50 exhibited superior accuracy, particularly for testing with large datasets. The automation of brain MRI image segmentation was tackled in another study (reference [46]), which employed a CNN model. Tumor detection in brain images was investigated through a CNN model in reference [47], with evaluation metrics such as Sensitivity, Specificity, and Precision. Incorporating both MRI and CT scan images, reference [48] employed a CNN for brain image classification and employed the Fuzzy C-Means clustering algorithm for segmentation. An automated brain

tumor detection system was presented in reference [52], utilizing CNN with specialized small-weight kernels. Another study (reference [53]) explored the classification of common brain tumor types (Glioma, Meningioma, and Pituitary) via a CNN architecture with layers for convolution, max-pooling, flattening, and a hidden layer.

Beyond brain-related applications, skin disease diagnosis was automated using a CNN in reference [49], involving image filtering, feature extraction, and classification. Additionally, CNNs were employed for chest disease diagnosis in reference [50]. Shifting the focus to breast cancer detection using mammogram images, a study (reference [37]) proposed a CNN model tailored for feature extraction. This approach integrated a Region Proposal Network (RPN) and adopted a Region of Interest (ROI) strategy to identify breast mass abnormalities. Likewise, in another work (reference [55]), a CNN-based model was introduced for detecting breast cancer in mammogram images, categorizing findings as normal, benign, or malignant.

Melanoma, a dangerous skin cancer, was the focus of [57], which proposed a two-stage method for automatic detection using Gaussian filtering, contour extraction, morphology, and ABCD rule-based feature extraction. [58] employed ABCD rule, GLCM, and HOG for feature extraction after image pre-processing and geodesic active contour (GAC) segmentation. [59] utilized PH2 database for melanoma detection, featuring pre-processing, multilevel thresholding-based segmentation, ABCD rule-driven feature extraction, and Total Dermatoscopic Value (TDV) for classification. [60] introduced a three-stage method using adaptive principal curvature, colour normalization, and ABCD rule for ISIC dataset-based melanoma detection. [61] proposed morphological filtering and thresholding for pre-processing, ABCD rule-based feature extraction, and classification of melanoma. [62] detailed image pre-processing, segmentation through ANCD rule, and neural network-based classification for melanoma detection. In [63], a segmentation-based approach fed into ABCD rule-driven feature extraction and Neural Network classification was proposed. [64] featured ABCD rule-driven feature extraction and ANN with Back Propagation for medical image processing involving melanoma detection. [65] incorporated unsupervised segmentation methods into feature extraction through ABCD rule, while [66] employed Watershed Segmentation, Wavelet Transformation, and Fuzzy Inference System-based classification for skin cancer detection and analysis.

III. METHODOLOGY

This section describes about the methods that are proposed. The details about the datasets and the proposed methods are described below.

1. **Database:** There are different datasets used in the proposed methods, which are collected from different sources. Chest X-ray, Brain cancer, Breast cancer, liver disorder, skin cancer are such datasets used in the work. The chest X-ray images are collected from Kaggle [73]. This dataset is having 5,863 X-Ray images and the images are in JPG format.

   The UCI machine learning repository [34] is a reputable source from which the breast cancer, brain tumor, and liver disorder datasets are sourced. These datasets are readily accessible online and are recognized in the field. They encompass medical data

with varying features, instances, and classes. The data within each dataset is split into training and testing sets. Each dataset is composed of two classes: cancerous (malignant) and non-cancerous (benign). These datasets differ in terms of their features and instances. The datasets consist of statistical features primarily extracted from images of cancerous conditions. For instance, the breast cancer dataset comprises 32 distinct features such as mean radius, mean texture, mean perimeter, and so forth. Similarly, the brain tumor dataset encompasses 11 features, including Clump Thickness, Uniformity of Cell Size, and Uniformity of Cell Shape. Lastly, the liver dataset contains 11 features such as Total Bilirubin and Alamine_Aminotransferase. These features have been sourced from the UCI machine learning repository [34] and have been corroborated accordingly.

The study utilized the BRATS [72] open access resource to obtain an MRI image dataset for brain tumors. This dataset consisted of 2065 images that were employed for experimental purposes. Out of these images, 1085 were categorized as abnormal, indicating the presence of tumors, and were labeled as "yes." The remaining approximately 980 images were categorized as normal, representing regions without tumors, and were labeled as "no." The dataset was split into training and testing subsets, with 80% of the data used for training and the remaining 20% for testing. This division resulted in 1652 images for training and 413 images for testing. Within the training dataset, there were 878 tumor images and 774 non-tumor images. In the testing dataset, there were 207 tumor images and 206 non-tumor images. The training data was further divided into training and validation sets using an 80:20 ratio.

The dermoscopy images for skin cancer were obtained from the ISIC 2020 (International Skin Imaging Collaboration) repository, a renowned open-source resource. This dataset comprised two groups of cancer images: benign lesions and malignant lesions. It encompassed 10,982 images for testing and 33,126 images for training. To address the absence of ground truth for testing images, the training dataset was divided into an 80:20 ratio for training and testing purposes. All images in this dataset were in JPG format. Within the total of 33,126 input images, 32,542 were categorized as benign, while 584 were designated as malignant.

2. **Preprocessing:** The initial step of the proposed approach involves preprocessing the input dataset to eliminate undesired elements such as artifacts, low contrast, hairs, veins, skin colors, and moles from the input images. This preprocessing phase comprises the following operations:

Filtering:

- **Median Filtering:** Among various techniques in biomedical image processing, the median filter stands out as the most commonly utilized method. It is straightforward to apply and tends to yield superior outcomes compared to other filtering methods. Noise present in medical images can significantly degrade image quality, which poses challenges for tasks like segmentation and classification. Therefore, noise reduction is crucial for achieving accurate results. Median filtering involves sorting the values within a window and replacing the center pixel with the middle value, effectively mitigating noise to some degree.

- **Adaptive Median Filter:** To overcome the limitations associated with the conventional median filter, a novel technique known as adaptive median filtering is introduced. This method offers several advantages by employing a variable-sized kernel around the distorted image, leading to an enhanced output quality. An important distinction between the adaptive filter and the median filter lies in how they treat pixel values. Unlike the median filter, which replaces all pixel values with the computed median, the adaptive filter takes a different approach.

The adaptive filtering process unfolds in two sequential steps. Initially, it calculates the median value within the kernel's range. Subsequently, it evaluates whether the present pixel value indicates the presence of impulsive noise, commonly referred to as salt and pepper noise. The detection of this noise relies on two fundamental assumptions. First, it considers a clean image to consist of smoothly transitioning areas interspersed with edges. Second, it assumes that noisy pixels typically exhibit exceedingly high or extremely low grayscale values when compared to their neighboring pixels.

In contrast to the spatially fixed 3 × 3 filter size used in the standard median filter, the adaptive median filter adapts its kernel size based on the specific image region. Typically, both dimensions of the filter are odd. Given an input image I, the resulting filtered image f is defined by this process.

$$f(x, y) = \text{median}\ \{I(s, t) \qquad (1)$$

In equation (1), (x, y) are the coordinates of the pixel in the contextual region W_{xy} specified by 3×3, and (s, t) are the coordinates of the pixels in that region.

The Method is Followed by the Steps:

- Step 1: Start by using a 3×3 filtering window as a starting point.
- Step 2: Within the current filtering window, determine the count of pixels identified as containing noise and those that are noise-free.
- Step 3: Verify whether the central area is corrupted or intact.
- Step 4: If the count of uncorrupted pixels within the filtering window is less than half of the total pixel count in the window, proceed to step 5.
- Step 5: Incrementally increase the window's size outward by one pixel on all four corners of the window.

Repeat the above steps if the specified condition is not met.

Hence, the present pixel will be excluded from the filtering operation as it has been categorized as noisy. The median filtering method solely employs pixels marked as clean from noise within the filtering window. This approach leads to enhanced filtering outcomes with reduced distortion. The intricate design of the suggested adaptive median filter is outlined in Figure 1.

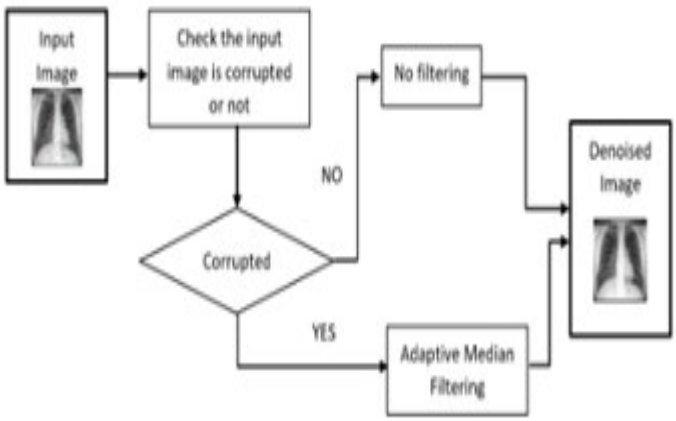

Figure 1: Block diagram of the proposed Adaptive median filtering method

- **Hair Removal:**Unwanted hairs present in skin cancer images can potentially interfere with the segmentation and feature extraction processes. Therefore, it is crucial to identify and eliminate these hairs from the images. To detect the presence of hair in the input images, we employed the Bottom Hat Filtering technique. Subsequently, the Fiber Metric Filtering method was applied to effectively eliminate the undesired hairs from the dataset.

IV. MORPHOLOGICAL METHOD

Morphology involves manipulating images based on their shapes. The alteration of the image, through addition or removal of pixels, depends on the size and shape of the structural element used. These operations are primarily applied to digital images. In the suggested approach, the morphological operator is utilized to eliminate minor objects from the original image, resulting in an improved output image.

V. SEGMENTATION

In the initial stage, the pre-processed image undergoes a process called segmentation. This step is crucial in identifying the precise location of the skin lesion. Segmentation holds significant importance in the analysis of medical images as it lays the foundation for accurate and efficient subsequent steps. Particularly in medical image analysis, segmenting images within regions of interest is essential. Segmentation involves classifying the pixels within an image into meaningful groups, a process known as semantic grouping. The primary aim of segmentation is to extract pertinent portions of the input image, simplifying the overall image analysis process. It serves to identify the boundary between the cancerous area and the surrounding tissues. Through this process, a binary mask is generated, highlighting the skin lesion.

In the study, the authors utilized the Otsu method for skin lesion segmentation. The Otsu method is an algorithm for global adaptive binarization threshold image segmentation. It selects the threshold for segmentation based on the highest interclass variance between the background and the target image. In essence, the OTSU method is synonymous with the

concept of using the threshold that achieves the greatest between-class variance. By considering the grayscale characteristics of the image, the method distinguishes between foreground and background. The discrepancy between these two segments is most pronounced when the optimal threshold is employed. The OTSU method employs the maximum inter-class variance as a benchmark, which is a widely accepted standard. Given that variance serves as a key indicator of even grayscale distribution, higher variance values signify greater disparities between the two ends of the distribution graph.

1. **Feature Extraction:** Feature extraction plays a crucial role in classification processes, particularly in the realm of disease classification using cancerous images. These images undergo feature extraction to derive statistical attributes, which form the basis of our classification efforts. While there exist numerous potential features to extract from an image, we specifically focus on statistical ones. Once features are extracted, they are subsequently subjected to optimization.

   Undoubtedly, feature extraction holds paramount significance as it enables the extraction of significant information from input images. Within the context of Computer-Aided Diagnosis (CAD) systems, the primary objective of feature extraction is to identify distinctive attributes within skin lesion images that can effectively differentiate between benign and malignant cases. The prevalence, effectiveness, efficiency, and straightforwardness of the feature extraction process have led many early detection systems for skin lesions to adopt an approach aligned with the ABCD rule for images. Employing computer algorithms, the capability of the ABCD rule to accurately capture critical features of malignant lesions—such as asymmetry, border irregularity, color variations, and diameter—can be evaluated.

   - **Asymmetry (A):** Asymmetry plays a crucial role in distinguishing between benign and malignant tumors. The central concept of asymmetry involves splitting an image into two equal halves and contrasting them to ascertain the tumor's nature. If the two halves exhibit similarity, the tumor is likely benign. Conversely, if dissimilarity exists, especially resulting in asymmetry, it suggests melanoma, a common asymmetrical malignancy.

   - **Border Irregularity (B):** The B factor assesses the edges of skin lesions. Melanoma may develop when the boundaries of a skin lesion appear uneven, notched, or unclear. The measure of border irregularity relies on four factors: variation, asymmetry, average and variation in image gradient, and image fractal properties.

   - **Color (C):** In instances of cancerous skin lesions, the pigmentation is often uneven, characterized by a lack of uniformity. To quantify this unevenness, it's essential to identify the potential existence of six distinct colors: white, black, red, blue, dark brown, and light brown. Each identified color contributes a value of 1 to the C factor calculation.

   - **Diameter (D):** Skin cancer cells proliferate more rapidly compared to surrounding cells, and their growth follows an exponential pattern. The diameter of a lesion plays a crucial role in distinguishing between melanoma and benign growths. Typically, melanoma lesions exhibit a diameter exceeding six millimeters.

2. Optimization

Brain Storm Optimization Algorithm (BSOA): BSO stands for Brainstorming-Inspired Optimization, a novel and advanced optimization algorithm [27] that draws inspiration from the brainstorming process of human idea generation. Brainstorming has proven effective in tackling intricate and complex problems. Compared to algorithms inspired by animal behaviors, those inspired by human processes tend to be more potent [28]. In BSO, a potential solution is denoted as a vector with 'D' dimensions, corresponding to the problem's complexity. The algorithm employs k-means clustering, initially generating 'N' random solutions within the search space, which are then organized into 'M' clusters. The fittest solution from each cluster becomes the cluster center [24]. In each iteration, new solutions are created either by modifying existing solutions or by combining two solutions from different clusters. Refer to Figure 2 for the pseudocode outlining the proposed BSO algorithm.

Brain Storm Optimization Algorithm

1. **Initialization**
2. Randomly generate N ideas (1<=i<=N) potential solutions (individuals)
3. **While (Not Stop) Do**
4. The k-means method divides the population into M clusters.
5. Record the best idea in each cluster as the cluster centre.
6. r =rand (0,1)
7. **if** *rand* (0, 1) < $p_{replace}$ **then**
8. Select a cluster and replace a random cluster centre with a new random solution.
9. **end** of **if**
10. **for (i=1 to N)**
11. Create new solutions.
12. r =rand (0,1)
13. **if** ($r < p_{one}$) *then*
14. Select a cluster c_x with probability of p_{cx}.
15. r_1=rand (0,1)
16. **if** ($r_1 < p_{one\_center}$) **then**
17. Change the c_x cluster centre by adding random value.
18. **Else**
19. Change a random solution from the *cx* by adding random value.
20. **end if**
21. **else**
22. Select two random clusters.
23. r_2=rand (0,1)
24. **if** $r_2 < p_{two\_center}$ **then**
25. New solution is the combination of two cluster centres.
26. **Else**
27. New solution is the combination of two random solutions from the selected clusters.
28. **end if**
29. **end if**
30. Keep better solution between old and new one.
31. **End of for** *n* new solution is generated.
32. **End of While** iteration number equal to maximal iteration number
33. **End**

Figure 2: Pseudo code of the BSOA

The probability p_{one} is the probability of one solution i.e., x_{old} which is an old one and can be replaced by the new one. The new solution is represented as x_{new} and described in equation (2),

$$x^{i}_{new} = x^{i}_{old} + \zeta(t) * \text{rand}() \quad (2)$$

Where,

rand() – it is a randomly generated distributed value, which range from 0 to 1.

x^{i}_{new}, x^{i}_{old} – i_{th} dimension of x_{new} , x_{old}

ζ represented as a constant value for controlling the random values. It is derived in equation (3):

$$\zeta(t) = \text{logsig}\left(\frac{0.5\times T-t}{k}\right) \times \text{rand}() \quad (3)$$

Here,
T - max no. of iterations
t - current iteration
k - coefficient to change logsig () (logarithmic sigmoid transfer function) function's slope

Here, the parameter p_{cx} of BSO algorithm from the pseudo code is directly proportional to the number of possible solutions present inside the cluster and it's equal to the probability of selecting a cluster from which the solution will be derived. The parameters p_{one_center} and p_{two_center} of the method describes the probability of choosing the centre of the cluster or the random values from a given cluster. When there will be a combination of two solutions is taken place (with probability $1 - p_{one}$), the resultant solution will contain the average of the two solutions that are selected before. When a new random solution is created, the exploration is carried out in the BSO algorithm and that will replace the centre of the cluster with probability $p_{replace}$.

3. Classification

- **Support Vector Machine:** The support vector machine (SVM) stands out as a widely recognized and efficient machine learning technique employed for classification tasks. Functioning within the realm of supervised learning, SVM scrutinizes datasets with the intention of carrying out classification. Its applications span across diverse domains, including the medical field where it finds utility in tasks such as disease classification and detection. Notably, SVM [23] enjoys employment across numerous sectors. In the scope of this study, we harnessed SVM as a classifier to categorize input features. To bolster SVM's performance, we incorporated a pipeline process. In instances where the dataset resides in a space characterized by high dimensions, SVM fabricates a hyperplane that serves the purpose of classification.

  Let us consider, 'Y_N' is the 'N' labelled data points in an 'H'-dimensional hyperspace. So, it is defined in equation (4):

  $$Y_N = [(x_1, d_1), \ldots., (x_N, d_N)] \square (X \times D)^N \quad (4)$$

  Where X is represented as the input space
  D represented as the label space (-1, +1)

  To design a random function Ψ, the problem statement is formulated:
  $\Psi: X \rightarrow D$ It calculates the value of d from x.

  The hyperplane described by (w, b) in the feature space as,

  $$\sum_{j=0}^{q} w_j \emptyset_j(x) + b = 0 \quad (5)$$

  Here ϕ is the mapping function.

SVM employs diverse kernel functions, with a particular emphasis on four: RBF, linear, polynomial, and sigmoid. Among these, RBF stands out as the most frequently utilized kernel. These kernel functions calculate the inner product between two points within a designated feature space. In our study, RBF consistently delivers superior accuracy compared to the other three options.
Kernel function:

$$K = \begin{matrix} 1 \\ 0 \end{matrix} \text{ if} \quad (6)$$

- **Linear Kernel Function**: This kernel is the most essential building block, and it becomes particularly valuable when dealing with a multitude of features that require analysis. It outperforms all other kernels in terms of speed and has a one-dimensional characteristic. The formula for this kernel is provided in equation (7).

$$F(x, xi) = sum(x. xi) \quad (7)$$

In this case, x, xi represents the data for classification.

- **Polynomial Kernel Function:** This particular kernel isn't widely recognized due to its inefficiency and imprecise assessment. It is essentially a variation of the linear kernel function, expanded upon. The mathematical depiction of this kernel can be found in equation (8).

$$F(x, xi) = (x. xi+1)\ ^d \quad (8)$$

Here '.' Represents the dot product
'd' is the degree

- **Sigmoid Kernel:** Generally, it is used in neural networks. It is related to the two-layered perceptron neural network model that acts as an activation function for neurons.

$$F(x, xi) = tanh(\alpha x^T y + c) \quad (9)$$

- **Radial Basis Function (RBF):** This is commonly used and desired kernel function in SVM. It is very helpful when we don't have much knowledge about the dataset and is typically used with non-linear datasets. The required equation of the RBF function is given in equation (10):

$$F(x, xi) = exp(-gamma * ||x - xi||^2) \quad (10)$$

Gamma can range between 0 and 1. Gamma of 0.1 is the most desired value.

- ***Convolutional Neural Network (CNN):*** A Convolutional Neural Network (CNN) consists of neurons with adjustable weights and biases, capable of receiving inputs. CNN is a specialized neural network with multiple hidden layers, characterized by its hierarchical structure. These layers include convolutional, rectified linear unit (ReLU), input, output, pooling, normalization, and fully connected layers. Unlike other approaches, CNN stands out due to its numerous layers and unique activation

functions. It leverages techniques like convolution and pooling to learn pixel correlations within input images, capturing significant features. Our objective was to create a model for accurately diagnosing tumors from 2D Brain MRI images. CNN was chosen due to its sparse connectivity and parameter sharing properties, which are well-suited for this task. Although a fully connected neural network could also identify tumor regions, we opted for CNN's advantages.

The model comprises six CNN layers, each containing a 2D convolutional layer, MaxPooling, and batch normalization. The layer sizes are 32, 64, 128, 256, 256, and 256 respectively. Using a kernel size of 3 × 3 and MaxPooling of 2 × 2, the ReLU activation function is applied throughout these layers. To enhance parameter learning, batch normalization is incorporated into the model. The subsequent section provides a comprehensive explanation of the activation functions utilized within the model.

- ***Rectified linear units (Relu):*** ReLU has become the prevailing activation function across various research domains today, finding application in nearly all deep learning and convolutional neural network models. It outperforms alternative activation functions such as tanh and sigmoid.

  The mathematical form of the Rectified Linear Unit (ReLU) is expressed in Equation (11).

$$F(y) = max(0, y) \tag{11}$$

  Where, $F(y) = 0, if y < 0$ And $F(y) = y, y \geq 0$

- ***SoftMax:*** The SoftMax activation function is widely utilized in deep learning applications, commonly placed in a neural network's final layer for output normalization. Its purpose is to transform numerical outputs into a probability distribution, yielding a vector as the result. The mathematical representation of the SoftMax function is provided in Equation (12).

$$F(y)_i = \frac{e^{y_i}}{\sum_{j=1}^{n} e^{y_j}} \tag{12}$$

  Where, y = The vector given as input to the SoftMax function F.
  y_i = i_{th} element of the input vector (any real value: positive, zero, or negative)
  e^{y_i} = the standard exponential function applied to the input vector
  $\sum_{j=1}^{n} e^{y_j}$ = It is a normalization term
  n = number of classes

- ***Batch normalization:*** Batch normalization is in charge of normalizing the output from the preceding layer. The application of batch normalization can improve the training process significantly. Its utilization aids in preventing overfitting. Equation (13) symbolizes the mathematical expression of batch normalization.

$$x^N = \left(\frac{x - p_x}{q_x}\right) \tag{13}$$

where, p_x = The average of the resulting output.
q_x = the output's measure of dispersion represented by the standard deviation

The suggested architecture involves a flatten layer that transforms the input data's dimensions to match the model's requirements. The model incorporates two dense layers which utilize ReLU and SoftMax activation functions. To mitigate overfitting, a dropout layer with a rate of 0.5 is included. The loss is computed using "sparse categorical cross-entropy" within the loss function. The optimization is carried out using the ADAM optimizer. The architecture of the proposed model shown in Figure 3 and the flow diagram of the proposed model is showcasing in Figure 4.

```
Model: "sequential"
_________________________________________________________________
Layer (type)                 Output Shape              Param #
=================================================================
conv2d (Conv2D)              (None, 254, 254, 32)      896
_________________________________________________________________
max_pooling2d (MaxPooling2D) (None, 127, 127, 32)      0
_________________________________________________________________
batch_normalization (BatchNo (None, 127, 127, 32)      128
_________________________________________________________________
conv2d_1 (Conv2D)            (None, 125, 125, 64)      18496
_________________________________________________________________
max_pooling2d_1 (MaxPooling2 (None, 62, 62, 64)        0
_________________________________________________________________
batch_normalization_1 (Batch (None, 62, 62, 64)        256
_________________________________________________________________
conv2d_2 (Conv2D)            (None, 60, 60, 128)       73856
_________________________________________________________________
max_pooling2d_2 (MaxPooling2 (None, 30, 30, 128)       0
_________________________________________________________________
batch_normalization_2 (Batch (None, 30, 30, 128)       512
_________________________________________________________________
conv2d_3 (Conv2D)            (None, 28, 28, 256)       295168
_________________________________________________________________
max_pooling2d_3 (MaxPooling2 (None, 14, 14, 256)       0
_________________________________________________________________
batch_normalization_3 (Batch (None, 14, 14, 256)       1024
_________________________________________________________________
conv2d_4 (Conv2D)            (None, 12, 12, 256)       590080
_________________________________________________________________
max_pooling2d_4 (MaxPooling2 (None, 6, 6, 256)         0
_________________________________________________________________
batch_normalization_4 (Batch (None, 6, 6, 256)         1024
_________________________________________________________________
conv2d_5 (Conv2D)            (None, 4, 4, 256)         590080
_________________________________________________________________
max_pooling2d_5 (MaxPooling2 (None, 2, 2, 256)         0
_________________________________________________________________
batch_normalization_5 (Batch (None, 2, 2, 256)         1024
_________________________________________________________________
flatten (Flatten)            (None, 1024)              0
_________________________________________________________________
dense (Dense)                (None, 255)               261375
_________________________________________________________________
dropout (Dropout)            (None, 255)               0
_________________________________________________________________
dense_1 (Dense)              (None, 2)                 512
=================================================================
Total params: 1,834,431
Trainable params: 1,832,447
Non-trainable params: 1,984
_________________________________________________________________
```

Figure 3: Architecture of Proposed CNN model

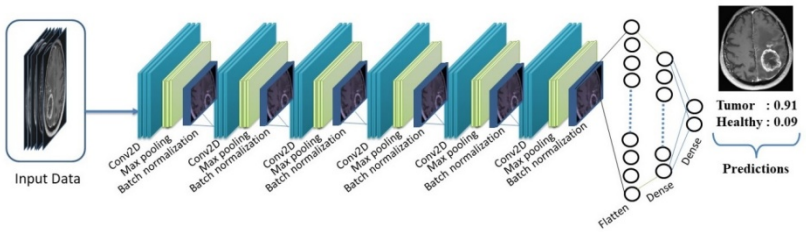

Figure 4: Flowchart illustrating the suggested CNN architecture.

- **KNN (k-nearest neighbours):** K-Nearest Neighbors (KNN) stands out as the most straightforward and user-friendly classifier when compared to other classification methods. This classifier operates by determining the class of a

data point based on the nearest distances to other data points in the training set. When both the training and testing data are fed into the classifier, it computes the distance to each class. The characteristics derived from the initial feature extraction step serve as inputs to the KNN algorithm for the purpose of classification.

- **Random Forest:** Random forest is a machine learning technique employed for image classification. It operates as an ensemble model, leveraging outcomes from other models to generate its own predictions. It's observed that ensemble models often outperform standalone models, as evidenced by various instances.

VI. RESULT

1. **Proposed Adaptive Median Filter:** An adaptive median filter was developed using Python 3 on a Windows OS platform to address noise issues. The efficiency of the filter was assessed using PSNR (peak signal to noise ratio) values, where higher PSNR values indicate better noise reduction.

The provided images demonstrate the outcomes of employing the adaptive median filter on an X-ray chest image with varying levels of noise, ranging from 10% to 50%. Figure 5 presents the sequence: the original chest X-ray, the same image with minimal noise (10% noise level), and the outcome following the application of the adaptive median filter on the noisy image. This result closely resembles the original image.

Similarly, Figure 6 depicts the original chest X-ray, a noisy counterpart with 20% noise, and the denoised image resulting from the filter application. This pattern is maintained in Figures 7, 8, and 9, each illustrating the steps of applying the filtering technique. Notably, the noise being addressed in the noisy images is salt and pepper noise.

(i) (ii) (iii)

Figure 5: Column (i) displays the initial chest X-ray image. In column (ii), the image is presented with 10% noise added, and in column (iii), the image is showcased after applying the adaptive median filter for the purpose of denoising.

(i) (ii) (iii)

Figure 6: Column (i) displays the initial chest X-ray image. In column (ii), the image is presented with 20% noise added. Column (iii) demonstrates the application of the adaptive median filter for denoising the image.

(i) (ii) (iii)

Figure 7: Column (i) displays the initial chest X-ray image. Column (ii) presents the same image but with a 30% noise addition. Column (iii) exhibits the image after applying the adaptive median filter for noise reduction.

(i) (ii) (iii)

Figure 8: Column (i) displays the initial chest X-ray image. Column (ii) depicts the same image but with an additional 40% noise added. Column (iii) presents the denoised version of the noisy image achieved through the application of an adaptive median filter.

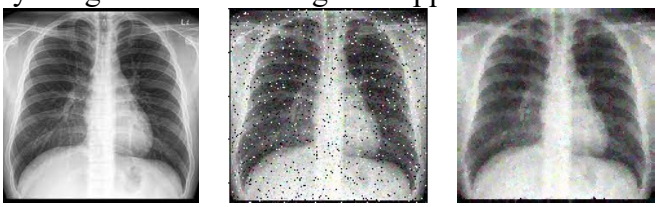

(i) (ii) (iii)

Figure 9: Column (i) displays the initial chest X-ray image. In column (ii), the image is presented with 50% noise added to it. Column (iii) showcases the image after employing the adaptive median filter for the purpose of denoising.

Noise densities in the images are varied from 10% to 50%, and their Mean Squared Error (MSE) and Peak Signal-to-Noise Ratio (PSNR) are computed. It's important to highlight that a higher PSNR and a lower MSE indicate the superiority of the filtering method. The outcomes are organized in tabular format in the Table 1 provided below.

Table 1: PSNR Values for medical image at different noise densities.

Noise Percentage	Adaptive Median Filter (PSNR)
10%	33.6507 dB
20%	32.7506 dB
30%	32.3798 dB
40%	31.9462 dB
50%	31.7087 dB

2. **Support Vector Machine with Optimized Statistical Features:**: In this study, we employed the Brain Storm Optimization algorithm to optimize three distinct datasets: Breast Cancer, Brain Tumor, and Liver Disorder. Our choice of the Brain Storm Optimization algorithm stemmed from its demonstrated effectiveness. To improve the accuracy of our classifiers, we adopted a pipelining approach with Support Vector Machines (SVM). Support Vector Machines offer various kernel options, including linear, polynomial, radial basis function (RBF), and sigmoid. For our analysis, we evaluated these four kernels by applying them to the three medical datasets. The results, as presented in Table 2, indicate that the radial basis function (RBF) kernel outperforms the others in terms of accuracy.

Table 2: Detailed overview of the Kernels

	Kernel Based			
Dataset	RBF	Linear	Poly	Sigmoid
Breast Cancer	98%	96%	90%	95%
Brain Tumour	99%	98%	96%	97%
Liver Disorder	91%	88%	85%	87%

We implemented the suggested approach across several methods outlined in the literature review. Our proposed method demonstrated superior accuracy compared to other cutting-edge techniques. When applied to the Breast cancer dataset, the optimized SVM achieved a remarkable accuracy of 98%. Similarly, the Brain tumor dataset saw a significant improvement with an accuracy of 99%, while the liver dataset exhibited a notable 91% accuracy using the RBF kernel. Among the kernels explored in this study, the Polynomial kernel yielded the least accuracy, trailing behind the other three kernels. The outcomes of the experimentation are presented in Table 3, showcasing the results obtained from the state-of-the-art methods.

Table 3: Details about the Accuracy and the different methods

Breast Cancer		**Brain Tumour**		**Liver Disorder**	
Method	**Accuray**	**Method**	**Accuray**	**Method**	**Accuray**
ABCFS + SVM	95%	ABCFS + SVM	96.5%	ABCFS + SVM	80%

BSO + SVM	96%	BSO + SVM	97.5%	BSO + SVM	81.31%
MBSO + SVM	98%	MBSO + SVM	99%	MBSO + SVM	86%

3. **Proposed CNN Model:** The researchers introduced a model designed for classifying brain tumors based on Brain MRI images, with the aim of predicting whether a tumor is benign or malignant. The model they proposed demonstrated a high accuracy of 98.5% after undergoing 50 epochs of training. To assess the model's effectiveness, they calculated various parameters such as accuracy, precision, recall, F-score, sensitivity, and specificity, as outlined in equations (14) to (19).

$$Accuracy = \frac{TP+TN}{TP+TN+FP+FN} \times 100 \quad (14)$$

$$Precision = \frac{TP}{TP+FP} \times 100 \quad (15)$$

$$Recall = \frac{TP}{TP+FN} \times 100 \quad (16)$$

$$F1Score = 2 \times \frac{Recall \times Precision}{Recall+Precision} \times 100 \quad (17)$$

$$Sensitivity = \frac{TP}{TP+FN} \times 100 \quad (18)$$

$$Specificity = \frac{TN}{TN+FP} \times 100 \quad (19)$$

Following the experiment, we obtained the numerical values for these parameters, as detailed in TABLE 4.

Table 4.: Evaluating Parameters

Precision	99.51%
Recall	99%
F-score	98.56%
Sensitivity	97.62%
Specificity	99.51%
Accuracy	98.55%

The graph in Figure 10 illustrates the accuracy of the proposed model across epochs, with the X-axis depicting accuracy and the Y-axis depicting the number of epochs.

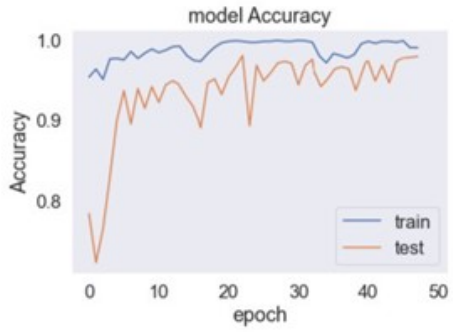

Figure 10: Graph depicting Accuracy during Training and Testing

The results of the suggested model are depicted in Figure 11.

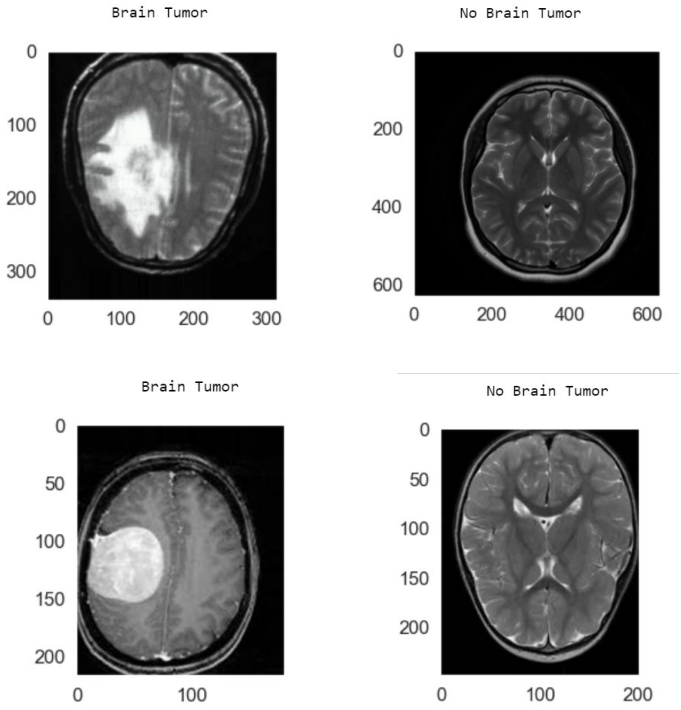

Figure 11: Resulting image output along with its predicted label.

The effectiveness of the suggested model's performance is also demonstrated through the utilization of the confusion matrix, illustrated in Figure 12.

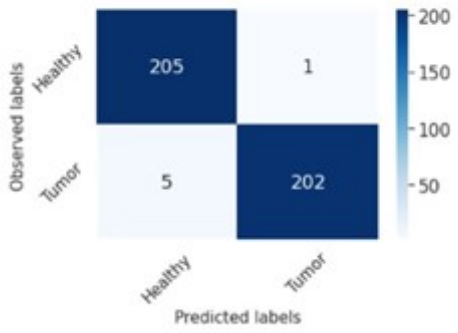

Figure 12: confusion matrix for the model we have introduced

The data presented in Figure 12 showcase the precision of the model in its classification task. This is evident from its remarkable high values for true positives (TP) and true negatives (TN). On the other hand, the instances of false positives (FP) and false negatives (FN) are quite rare, which highlights how well the model's strategy is performing.

As demonstrated in the provided TABLE 5, our novel CNN model has exhibited remarkable accuracy when contrasted with contemporary methods discussed in the literature review. Our proposed model has achieved an impressive accuracy rate of 98.5%. This outcome underscores the evident superiority of our CNN model over alternative CNN models in terms of performance evaluation.

Table 5: Contrast the suggested approach with alternative methods.

Model	**Accuracy**
DCNN+WCA	97.23%
DCNN+ Back Propagation	95.43%
FCM + CNN	91%
FCNN	98.3%
3 Layered CNN	96.08%
CNN Model	97.87%
CNN method	97.5%
Proposed Modified CNN	98.5%

4. **Proposed machine learning techniques with ABCD features:**: Our proposed technique aims to differentiate between benign and malignant images using input data. To enhance the accuracy of our results, we apply several pre-processing steps to the input image.

The gray-scale picture is subjected to a median filtering technique to eliminate undesired noise from the image. The result of this filtering process is depicted in Figure 13.

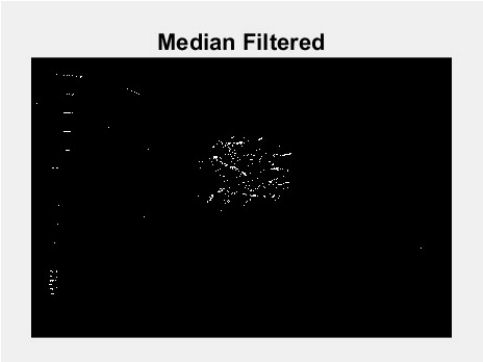

Figure 13: Applied median filter

Unwanted hair present in input images was effectively eliminated using Fiber Metric Filtering. The outcomes of this approach can be observed in Figure 14.

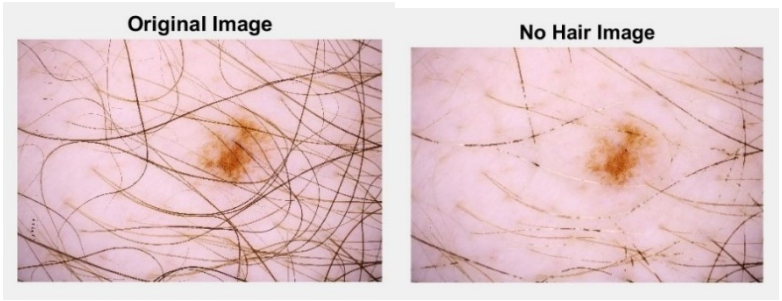

(a) (b)

Figure14: (a) The image in its original state, (b) The image with the hair removed

Segmentation using the Otsu method is performed on the pre-processed image as a crucial step in the process of detecting skin cancer. The Otsu method is utilized to process the image, and the resulting output is displayed in Figure 15.

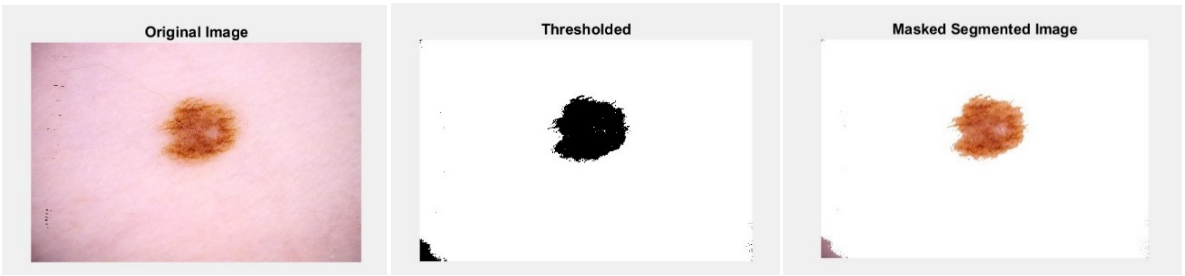

(a) (b) (c)

Figure 15 (a) The initial picture, (b) The image with thresholding applied, (c) The image where segmentation is restricted by a mask.

The extracted features from the segmented image are obtained using the ABCD rule, as illustrated in Figure 17. A closer look at the extracted features is provided in Figure 18. In this figure, the various colors within the cancerous image are displayed. It is evident from Figure 18 that the red color indicates the presence of cancerous regions.

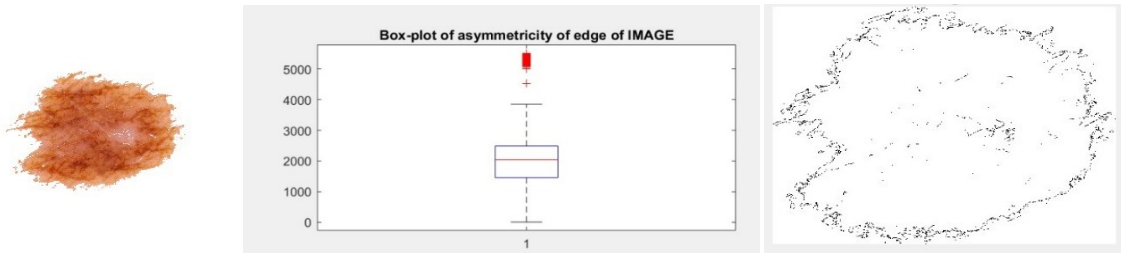

(a) (b) (c)

Figure 17: (a) The initial picture, (b) Graphical representation displaying the unevenness of the tumor edge, (c) Outline of the cancerous region.

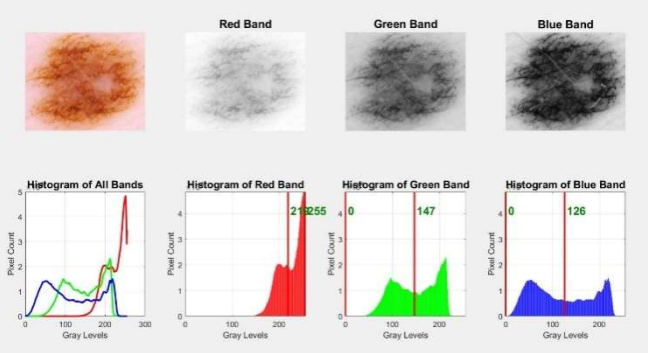

Figure 18: Histogram for each individual color channel

The final stage involves classifying the extracted features using various machine learning algorithms to identify whether the part is benign or malignant. The authors utilized Support Vector Machine (SVM), k-Nearest Neighbors (KNN), and Random Forest (RF) for this classification task. Among these classifiers, SVM exhibited the highest performance with an accuracy of 94.01%. In contrast, KNN achieved an accuracy of 91.2%, while RF yielded an accuracy of 90.9%. The specific numerical results from this classification step can be found in TABLE 6.

Table 6: Performance outcomes of various classifiers in terms of accuracy

Classifier	**Accuracy**
SVM	93.51%
KNN	91%
Random Forest	90.67%

The accuracy achieved from the experiment is supported by the confusion matrices depicted in Figures 19, 20, and 21.

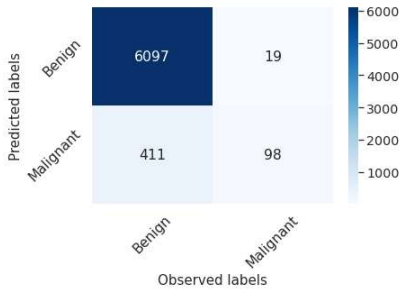

Figure 19: Confusion matrix of Support Vector Machines (SVMs).

Figure 20: Confusion matrix of K-Nearest Neighbors (KNN)

Figure 21: Confusion matrix pertaining to Random Forest.

VII. CONCLUSIONS

Medical imaging refers to acquiring images from a living organism's body for medical reasons, like disease detection and analysis. Cancer-related datasets go through several stages and are ultimately categorized using different machine and deep learning algorithms. Among these, Convolutional Neural Networks (CNNs), a type of deep learning algorithm, achieve an accuracy of 98.5%. On the other hand, machine learning algorithms involve preprocessing, segmentation, and feature extraction steps before classification. Within these classifiers, Support Vector Machine (SVM) stands out with a 99% accuracy rate when utilizing optimized features.

REFERENCES

[1] Liu, Xiangbin, Liping Song, Shuai Liu, and Yudong Zhang. "A review of deep-learning-based medical image segmentation methods." Sustainability 13, no. 3 (2021): 1224.
[2] Kaur, Charnpreet, and Urvashi Garg. "Artificial intelligence techniques for cancer detection in medical image processing: A review." Materials Today: Proceedings (2021).
[3] Sagheer, Sameera V. Mohd, and Sudhish N. George. "A review on medical image denoising algorithms." Biomedical signal processing and control 61 (2020): 102036.
[4] Wang, Jian, Hengde Zhu, Shui-Hua Wang, and Yu-Dong Zhang. "A review of deep learning on medical image analysis." Mobile Networks and Applications 26, no. 1 (2021): 351-380.
[5] Shrestha, Suman. "Image denoising using new adaptive based median filters." arXiv pre-print arXiv:1410.2175 (2014).
[6] Gao, Zhongxin. "An Adaptive Median Filtering of Salt and Pepper Noise based on Local Pixel Distribution." In the 2018 International Conference on Transportation & Logistics, Information & Communication, Smart City (TLICSC 2018). 2018.

[7] Chang, Chin-Chen, Ju-Yuan Hsiao, and Chih-Ping Hsieh. "An adaptive median filter for image denoising." In 2008 Second International Symposium on Intelligent Information Technology Application, vol. 2, pp. 346-350. IEEE, 2008.
[8] Hwang, Humor, and Richard A. Haddad. "Adaptive median filters: new algorithms and re-sults." IEEE Transactions on image processing 4, no. 4 (1995): 499-502.
[9] Boateng, Kwame Osei, Benjamin Weyori Asubam, and David Sanka Laar. "Improving the effectiveness of the median filter." (2012).
[10] Ibrahim, Haidi, Nicholas Sia Pik Kong, and Theam Foo Ng. "Simple adaptive median filter for the removal of impulse noise from highly corrupted images." IEEE Transactions on Consumer Electronics 54, no. 4 (2008): 1920-1927.
[11] Mehta, Rachna, and N. Kumar Aggarwal. "Comparative Analysis of Median Filter and Adaptive Filter for Impulse Noise A Review." International Journal of Computer Applica-tions 975 (2014): 8887.
[12] Shrestha, Suman. "Image denoising using new adaptive based median filters." arXiv pre-print arXiv:1410.2175 (2014).
[13] Soni, Hetvi, and Darshana Sankhe. "Image Restoration using Adaptive Median Filter-ing." Image 6, no. 10 (2019).
[14] Dwivedy, Prashant, Anjali Potnis, and Madhuram Mishra. "Performance Assessment of Several Filters for Removing Salt and Pepper Noise, Gaussian Noise, Rayleigh Noise and Uniform Noise." Empirical Research Press Ltd. (2017): 176.
[15] Sathesh, A., and K. Rasitha. "A nonlinear adaptive median filtering-based noise removal algorithm." In Proceedings of First International Conference on Modeling, Control, Auto-mation and Communication (ICMCAC-2010), pp. 108-113. 2010.
[16] Panda, B., Nayak, S. K., & Mihir Narayan Mohanty (2021). Noise Suppression in Nonsta-tionary Signals Using Adaptive Techniques. In Advances in Electronics, Communication and Computing (pp. 261-270). Springer, Singapore
[17] Kar, P., & Mihir Narayan Mohanty (2020). An Intelligent Approach for Noise Elimination from Brain Image. In Advanced Computing and Intelligent Engineering (pp. 391-400). Springer, Singapore.
[18] Amlan Jyoti, Mihir Narayan Mohanty, Sidhant Kumar Kar, B. N. Biswal, “Optimized Clustering Method for CT Brain Image Segmentation”, Advances in Intelligent Systems and Computing, Springer International Publishing Switzerland, Volume 327, 2015, pp 317-324.
[19] Ashutosh Dehuri, Siba Sanyena, Rupeli Rupanita Dash, Mihir N. Mohanty, “A Compara-tive Analysis of Filtering Techniques on Application in Image Denoising”, IEEE Conf. CGVIS-2015, KIIT, Bhubaneswar, Odisha
[20] Keerthiveena, B., S. Esakkirajan, Badri Narayan Subudhi, and T. Veerakumar. "A hybrid BPSO-SVM for feature selection and classification of ocular health." IET Image Processing 15, no. 2 (2021): 542-555.
[21] Harb, Hany M., and Abeer S. Desuky. "Feature selection on classification of medical datasets based on particle swarm optimization." International Journal of Computer Applications 104, no. 5 (2014).
[22] Brezočnik, Lucija. "Feature selection for classification using particle swarm optimization." In IEEE EUROCON 2017-17th International Conference on Smart Technologies, pp. 966-971. IEEE, 2017.
[23] Mohanty, Mihir Narayan, Anurag Kumar, Aurobinda Routray, and Prithviraj Kabisatpathy. "Evolutionary algorithm-based optimization for power quality disturbances classification using support vector machines." International Journal of Control, Automation and Systems 8, no. 6 (2010): 1306-1312.
[24] Tuba, Eva, Ivana Strumberger, Timea Bezdan, Nebojsa Bacanin, and Milan Tuba. "Classification and feature selection method for medical datasets by brain storm optimization algorithm and support vector machine." Procedia Computer Science 162 (2019): 307-315.
[25] Hu, Xiao-Min, Shou-Rong Zhang, Min Li, and Jeremiah D. Deng. "Multimodal particle swarm optimization for feature selection." Applied Soft Computing 113 (2021): 107887.
[26] Li, Xiaohua, Jusheng Zhang, and Fatemeh Safara. "Improving the accuracy of diabetes diagnosis applications through a hybrid feature selection algorithm." Neural Processing Letters (2021): 1-17.
[27] Shi, Yuhui. "Brain storm optimization algorithm." In International conference in swarm intelligence, pp. 303-309. Springer, Berlin, Heidelberg, 2011.
[28] Zhan, Zhi-hui, Jun Zhang, Yu-hui Shi, and Hai-lin Liu. "A modified brain storm optimization." In 2012 IEEE Congress on Evolutionary Computation, pp. 1-8. IEEE, 2012.
[29] Omuya, Erick Odhiambo, George Onyango Okeyo, and Michael Waema Kimwele. "Feature selection for classification using principal component analysis and information gain." Expert Systems with Applications 174 (2021): 114765.

[30] Jyoti, Amlan, Mihir N. Mohanty, Sidhant Kumar Kar, and Bhabendra Narayan Biswal. "Optimized clustering method for CT brain image segmentation." In Proceedings of the 3rd International Conference on Frontiers of Intelligent Computing: Theory and Applications (FICTA) 2014, pp. 317-324. Springer, Cham, 2015.
[31] Sahoo, Debendra Kumar, Satyasis Mishra, and Mihir Narayana Mohanty. "Wavelet Transform and WCA Based Deep Convolutional Network for Brain Tumor Detection and Classification from Magnetic Resonance Images." PalArch's Journal of Archaeology of Egypt/Egyptology 17, no. 9 (2020): 2319-2328.
[32] Das, Abhishek, Saumendra Kumar Mohapatra, and Mihir Narayan Mohanty. "Design of deep ensemble classifier with fuzzy decision method for biomedical image classification." Applied Soft Computing 115 (2022): 108178.
[33] Das, Abhishek, Mihir Narayan Mohanty, Pradeep Kumar Mallick, Prayag Tiwari, Khan Muhammad, and Hongyin Zhu. "Breast cancer detection using an ensemble deep learning method." Biomedical Signal Processing and Control 70 (2021): 103009.
[34] Blake CL, Merz CJ. UCI repository of machine learning databases. Deparment of Information and Computer Sciences, University of California, Irvine, 1998, http://www.ics.uci.edu/□mlearn/mlrepository.html.
[35] Rao, L. Jagjeevan, Ramaiah Challa, Dorababu Sudarsa, Cherukuri Naresh, and CMAK Zeelan Basha. "Enhanced Automatic Classification of Brain Tumors with FCM and Convolution Neural Network." In 2020 Third International Conference on Smart Systems and Inventive Technology (ICSSIT), pp. 1233-1237. IEEE, 2020.
[36] Gurunathan, Akila, and Batri Krishnan. "Detection and diagnosis of brain tumors using deep learning convolutional neural networks." International Journal of Imaging Systems and Technology 31, no. 3 (2021): 1174-1184.
[37] Hadush, Simon, Yaecob Girmay, Abiot Sinamo, and Gebrekirstos Hagos. "Breast cancer detection using convolutional neural networks." arXiv preprint arXiv:2003.07911 (2020).
[38] Choudhury, Chirodip Lodh, Chandrakanta Mahanty, Raghvendra Kumar, and Brojo Kishore Mishra. "Brain tumor detection and classification using convolutional neural network and deep neural network." In 2020 International Conference on Computer Science, Engineering and Applications (ICCSEA), pp. 1-4. IEEE, 2020.
[39] Das, Abhishek, Mihir Narayan Mohanty, Pradeep Kumar Mallick, Prayag Tiwari, Khan Muhammad, and Hongyin Zhu. "Breast cancer detection using an ensemble deep learning method." Biomedical Signal Processing and Control 70 (2021): 103009.
[40] Das, Abhishek, and Mihir Narayan Mohanty. "Covid-19 detection from x-ray images using convolutional neural network." International Journal of Advanced Science and Technology 29, no. 8 Special Issue (2020).
[41] Das, Abhishek, Saumendra Kumar Mohapatra, and Mihir Narayan Mohanty. "Design of deep ensemble classifier with fuzzy decision method for biomedical image classification." Applied Soft Computing 115 (2022): 108178.
[42] Mohapatra, Saumendra Kumar, and Mihir Narayan Mohanty. "Convolutional Neural Network Based Arrhythmia Classification with Selective Features from Empirical Mode Decomposition." In Proceedings of the Second International Conference on Information Management and Machine Intelligence, pp. 375-383. Springer, Singapore, 2021.
[43] Sahoo, Debendra Kumar, Satyasis Mishra, and Mihir Narayana Mohanty. "Wavelet Transform and WCA Based Deep Convolutional Network for Brain Tumor Detection and Classification from Magnetic Resonance Images." PalArch's Journal of Archaeology of Egypt/Egyptology 17, no. 9 (2020): 2319-2328.
[44] Yadav, Samir S., and Shivajirao M. Jadhav. "Deep convolutional neural network based medical image classification for disease diagnosis." Journal of Big Data 6, no. 1 (2019): 1-18.
[45] Talo, Muhammed, Ozal Yildirim, Ulas Baran Baloglu, Galip Aydin, and U. Rajendra Acharya. "Convolutional neural networks for multi-class brain disease detection using MRI images." Computerized Medical Imaging and Graphics 78 (2019): 101673.
[46] Malathi, M., and P. Sinthia. "Brain tumor segmentation using convolutional neural network with tensor flow." Asian Pacific journal of cancer prevention: APJCP 20, no. 7 (2019): 2095.
[47] Siar, Masoumeh, and Mohammad Teshnehlab. "Brain tumor detection using deep neural network and machine learning algorithm." In 2019 9th International Conference on Computer and Knowledge Engineering (ICCKE), pp. 363-368. IEEE, 2019.

[48] Hossain, Tonmoy, Fairuz Shadmani Shishir, Mohsena Ashraf, MD Abdullah Al Nasim, and Faisal Muhammad Shah. "Brain tumor detection using convolutional neural network." In 2019 1st international conference on advances in science, engineering and robotics technology (ICASERT), pp. 1-6. IEEE, 2019.
[49] Rathod, Jainesh, Vishal Waghmode, Aniruddh Sodha, and Praseniit Bhavathankar. "Diagnosis of skin diseases using Convolutional Neural Networks." In 2018 Second International Conference on Electronics, Communication and Aerospace Technology (ICECA), pp. 1048-1051. IEEE, 2018.
[50] Abiyev, Rahib H., and Mohammad Khaleel Sallam Ma'aitaH. "Deep convolutional neural networks for chest diseases detection." Journal of healthcare engineering 2018 (2018).
[51] Mohsen, Heba, El-Sayed A. El-Dahshan, El-Sayed M. El-Horbaty, and Abdel-Badeeh M. Salem. "Classification using deep learning neural networks for brain tumors." Future Computing and Informatics Journal 3, no. 1 (2018): 68-71.
[52] Seetha, J., and S. Selvakumar Raja. "Brain tumor classification using convolutional neural networks." Biomedical & Pharmacology Journal 11, no. 3 (2018): 1457.
[53] Abiwinanda, Nyoman, Muhammad Hanif, S. Tafwida Hesaputra, Astri Handayani, and Tati Rajab Mengko. "Brain tumor classification using convolutional neural network." In World congress on medical physics and biomedical engineering 2018, pp. 183-189. Springer, Singapore, 2019.
[54] Amin, Javeria, Muhammad Sharif, Mussarat Yasmin, and Steven Lawrence Fernandes. "Big data analysis for brain tumor detection: Deep convolutional neural networks." Future Generation Computer Systems 87 (2018): 290-297.
[55] Tan, Y. J., K. S. Sim, and F. F. Ting. "Breast cancer detection using convolutional neural networks for mammogram imaging system." In 2017 International Conference on Robotics, Automation and Sciences (ICORAS), pp. 1-5. IEEE, 2017.
[56] Menze, Bjoern H., Andras Jakab, Stefan Bauer, Jayashree Kalpathy-Cramer, Keyvan Farahani, Justin Kirby, Yuliya Burren et al. "The multimodal brain tumor image segmentation benchmark (BRATS)." IEEE transactions on medical imaging 34, no. 10 (2014): 1993-2024.
[57] Senan, Ebrahim Mohammed, and Mukti E. Jadhav. "Analysis of dermoscopy images by using ABCD rule for early detection of skin cancer." Global Transitions Proceedings 2, no. 1 (2021): 1-7.
[58] Vidya, Maya, and Maya V. Karki. "Skin cancer detection using machine learning techniques." In 2020 IEEE International Conference on Electronics, Computing and Communication Technologies (CONECCT), pp. 1-5. IEEE, 2020.
[59] Zghal, Nadia S., and Nabil Derbel. "Melanoma skin cancer detection based on image processing." Current Medical Imaging 16, no. 1 (2020): 50-58.
[60] Thanh, Dang NH, V. B. Prasath, Le Minh Hieu, and Nguyen Ngoc Hien. "Melanoma skin cancer detection method based on adaptive principal curvature, colour normalisation and feature extraction with the ABCD rule." Journal of Digital Imaging 33, no. 3 (2020): 574-585.
[61] Lattoofi, Nabeel F., Israa F. Al-Sharuee, Mohammed Y. Kamil, Ayoob H. Obaid, Aya A. Mahidi, and Ammar A. Omar. "Melanoma skin cancer detection based on ABCD rule." In 2019 First International Conference of Computer and Applied Sciences (CAS), pp. 154-157. IEEE, 2019.
[62] Garg, Nishtha, Vishakha Sharma, and Prabhjot Kaur. "Melanoma skin cancer detection using image processing." In Sensors and Image Processing, pp. 111-119. Springer, Singapore, 2018.
[63] Dubal, Pratik, Sankirtan Bhatt, Chaitanya Joglekar, and Sonali Patil. "Skin cancer detection and classification." In 2017 6th international conference on electrical engineering and informatics (ICEEI), pp. 1-6. IEEE, 2017.
[64] Kanimozhi, T., and A. Murthi. "Computer aided melanoma skin cancer detection using artificial neural network classifier." Singaporean Journal of Scientific Research (SJSR), Journal of Selected Areas in Microelectronics (JSAM) 8, no. 2 (2016): 35-42.
[65] Bhuiyan, Md Amran Hossen, Ibrahim Azad, and Md Kamal Uddin. "Image processing for skin cancer features extraction." International Journal of Scientific & Engineering Research 4, no. 2 (2013): 1-6.
[66] Ramteke, Nilkamal S., and Shweta V. Jain. "ABCD rule based automatic computer-aided skin cancer detection using MATLAB." International Journal of Computer Technology and Applications 4, no. 4 (2013): 691.
[67] Mohanty, Mihir Narayan, Aurobinda Routray, Ashok Kumar Pradhan, and Prithviraj Kabisatpathy. "Power quality disturbances classification using support vector machines with optimised time-frequency kernels." International Journal of Power Electronics 4, no. 2 (2012): 181-196.
[68] Kumar, Anurag, Mihir N. Mohanty, and Aurobinda Routray. "Design of support vector machines with time frequency kernels for classification of EEG signals." In 2010 IEEE Students Technology Symposium (TechSym), pp. 330-333. IEEE, 2010.

[69] ITER, Siksha'O. "Corona Virus Infection Probability Classification using Support Vector Machine." (2020).
[70] Das, Abhishek, Saumendra Kumar Mohapatra, and Mihir Narayan Mohanty. "A Concatenated Model with Deep Learning Technique for Skin Lesion Detection." In 2021 5th International Conference on Information Systems and Computer Networks (ISCON), pp. 1-5. IEEE, 2021.
[71] Rotemberg, V., Kurtansky, N., Betz-Stablein, B., Caffery, L., Chousakos, E., Codella, N., Combalia, M., Dusza, S., Guitera, P., Gutman, D., Halpern, A., Helba, B., Kittler, H., Kose, K., Langer, S., Lioprys, K., Malvehy, J., Musthaq, S., Nanda, J., Reiter, O., Shih, G., Stratigos, A., Tschandl, P., Weber, J. & Soyer, P. A patient-centric dataset of images and metadata for identifying melanomas using clinical context. Sci Data 8, 34 (2021). https://doi.org/10.1038/s41597-021-00815-z
[72] Menze, Bjoern H., Andras Jakab, Stefan Bauer, Jayashree Kalpathy-Cramer, Keyvan Farahani, Justin Kirby, Yuliya Burren et al. "The multimodal brain tumor image segmentation benchmark (BRATS)." IEEE transactions on medical imaging 34, no. 10 (2014): 1993-2024.
[73] Kermany, Daniel; Zhang, Kang; Goldbaum, Michael (2018), “Labeled Optical Coherence Tomography (OCT) and Chest X-Ray Images for Classification”, Mendeley Data, V2, doi: 10.17632/rscbjbr9sj.2

